МИНЕРАЛОГИЧЕСКАЯ КРИСТАЛЛОГРАФИЯ

MECHANISMS OF PHASE TRANSITIONS BETWEEN AL_2SiO_5 POLYMORPHS

© 2021 г. A. I. Samtsevich[1, *] and A. R. Oganov[1, **]

[1]*Skolkovo Institute of Science and Technology, Skolkovo Innovation Center, Bolshoy Boulevard, 30, 1, Moscow, 121205 Russia*

**e-mail: A.Samtsevich@skoltech.ru*

***e-mail: A.Oganov@skoltech.ru*

Received May 26, 2021; Revised July 7, 2021; Accepted August 18, 2021

In nature Al_2SiO_5 exists as three polymorphs: kyanite, andalusite and sillimanite, often coexisting in the same rock. Here, we have studied in detail the mechanisms of structural transitions between all three phases of Al_2SiO_5 – kyanite-andalusite, andalusite-sillimanite and kyanite-sillimanite at the pressures of 0 and 10 GPa. The phase transition pathways with the lowest energy barriers are found by constructing a number of geometrically likeliest pathways and optimizing them using the variable-cell nudged elastic band method (VCNEB). We have analyzed the structural changes along the obtained lowest-energy pathways. These results have provided insights into the nature of structural relationships between Al_2SiO_5 polymorphs, their coexistence with each other and their transformation pathways. In particular, we confirm that phase transition barriers are very high, which allows these phases to coexist during geological timescales – thus serving as geothermobarometers.

Keywords: Al_2SiO_5 polymorphs, phase transitions mechanisms, density functional theory

DOI: 10.31857/S0869605521050051

INTRODUCTION

Minerals andalusite, kyanite and sillimanite are polymorphic modifications of Al_2SiO_5 (see Schmidt et al., 1997; Harben, 2002). Important for Earth sciences, they also have wide practical usage as ceramic and refractory materials (McMichael, 1990) and they are used to produce lightweight aluminum-silicon alloys for making metallic fiber, which in its turn is used in supersonic aircraft and spaceships, etc. (Skoog, Moore, 1988; Aryal et al., 2008; Belogurova, Grishin, 2012; Zhang et al., 2013). A closely related material, mullite, the main component of porcelain, has recently become a promising candidate for structural and functional ceramics due to its low thermal expansion, low thermal conductivity, and excellent creep resistance along with high-temperature strength and stability under severe chemical environments (Schneider, Komarneni, 2005; Schneider et al., 2008).

All three structures have some common features: all Si atoms are tetrahedrally coordinated and half of all Al atoms are in the octahedral coordination and form chains of edge-sharing AlO_6 octahedra (see Burnham, 1963; Ohuchi et al., 2006). The other half of Al atoms are in the tetrahedral coordination in sillimanite, 5-fold coordination in andalusite, and in the octahedral coordination in kyanite. Kyanite crystallizes in the triclinic system with space group $P\bar{1}$ (Yang et al., 1997b), while sillimanite and andalusite have orthorhombic structures with space groups *Pnnm* and *Pbnm*, respectively (Yang et al., 1997a, 1997b). All three polymorphs of Al_2SiO_5 are found commonly in metamorphic rocks and are geologically important markers since they provide information about pressure and temperature of their formation and the type of metamorphism (Atherton, Brotherton, 1974; Klein, Hurlbut, 1995; Whitney, 2002).

Andalusite is a low-pressure and low-temperature phase, while kyanite is formed at high pressures and low temperatures, and sillimanite is formed at medium or low pressures and high temperatures (Klein, Hurlbut, 1995; Kerrick, 2018). The entropies and Gibbs free energies of the three minerals are very similar (Klein, Hurlbut, 1995; Oganov et al., 2001).

In nature, often two or three polymorphs of Al_2SiO_5 are found coexisting in the same rock. There are numerous examples with each of two-polymorph assemblages, i.e. andalusite + kyanite, kyanite + sillimanite and andalusite + sillimanite (Evans, Berti, 1986; Lux et al., 1986; Pattison et al., 1991), and in many cases all three Al_2SiO_5 polymorphs coexist in a rock (Hietanen, 1956; Carey et al., 1992; Grover et al., 1992; Garcia-Casco, Torres-Roldan, 1996; Hiroi et al., 1998; Whitney, 2002; Sepahi et al., 2004; Gibson et al., 2004; Allaz et al., 2005; Sayab, 2006; Likhanov et al., 2009; Ali, 2010; Kim, Ree, 2010; Palin et al., 2012; Whitney, Samuelson, 2019; Baharfar et al., 2019; Gervais, 2019). Such coexistence indicates conditions of formation at a rock, corresponding to two- or three-phase equilibrium. Coexistence at normal conditions is due to high barriers of transitions, leading to metastable persistence of phases.

Numerous theoretical and experimental studies explored structural stability of different phases, the phase diagram, electronic and optical properties of Al_2SiO_5 phases. For example, Oganov and colleagues studied stable (Oganov, Brodholt, 2000) and metastable (Oganov et al., 2001) pressure-induced transitions. Zhu et al. predicted phase transition mechanisms between stable Al_2SiO_5 polymorphs using the evolutionary metadynamics method (Zhu et al., 2011), which is capable of giving crude atomistic mechanism, but not the kinetics of the transition.

Generally, transition state theory (TST) (Eyring, 1935) is used to estimate the reaction rate constants. A simplification to TST – the harmonic approximation – is most commonly used and transforms the kinetics estimation problem into another – seeking first-order saddle points on the complex multidimensional free energy surface (FES) and properties of this saddle point characterize the transition. One of the most popular techniques to study reaction paths is nudged elastic band (NEB) method (Jonsson et al., 1998; Henkelman et al., 2000; Henkelman, Jónsson, 2000), but the results of this method are highly dependent on the initial path. There are extensions of the NEB method allowing the study of solid-solid phase transitions, such as the solid-state NEB (SSNEB) (Caspersen, Carter, 2005), and in particular the generalized solid-state NEB (G-SSNEB) (Sheppard et al., 2012) and variable-cell NEB (VCNEB) (Qian et al., 2013).

Still, the search for the lowest-energy saddle point is not an easy task, especially for periodic systems – there are a huge (strictly speaking, infinite) number of possible initial paths (various atom-to-atom mappings and lattice-to-lattice mappings). The problem of mapping of crystal structures is essential for the initial path(s) generation. There are very few approaches that may help to do so, such as the algorithm developed by Stevanović and co-workers (Stevanović et al., 2018; Therrien et al., 2020) and the one developed by Munro et al. (2018), which are purely geometrical (dealing with mapping cell parameters and atomic positions, interatomic distances, angles, coordination polyhedra). However, the computational complexity of such methods grows exponentially with the number of atoms. Once a good initial approximation to the transition path is constructed, it can be refined by such methods as VCNEB or its analogs mentioned above.

Here we present a detailed study of the atomistic mechanisms of phase transitions between andalusite, sillimanite and kyanite.

METHODOLOGY

Initial structural models of the Al_2SiO_5 polymorphs were taken from experimental studies of Ralph et al. (Ralph et al., 1984) for andalusite and from Yang et al. (Yang et al., 1997a, 1997b) for kyanite and sillimanite. Then, these structures were relaxed. Structure relaxations and total energy calculations were performed using density functional theory (DFT) (Hohenberg, Kohn, 1964; Kohn, Sham, 1965) within the generalized gradient approximation (Perdew–Burke–Ernzerhof functional) (Perdew et al., 1996), and the projector augmented wave method (Blöchl, 1994; Kresse, Joubert, 1999) as implemented in the VASP (Kresse, Hafner, 1993, 1994; Kresse, Furthmüller, 1996) package. The plane-wave energy cutoff of 600 eV was

used, ensuring excellent convergence of total energies, forces and stresses. Crystal structures were relaxed until the maximum net force on atoms became less than 0.01 eV/Å. The Monkhorst–Pack scheme (Monkhorst, Pack, 1976) was used to sample the Brillouin zone, using $4 \times 3 \times 3$ meshes for all three Al_2SiO_5 phases.

Paths of phase transitions were optimized using the variable-cell nudged-elastic-band (VCNEB) method (Qian et al., 2013) as implemented in the USPEX code (Oganov, Glass, 2006; Oganov et al., 2010, 2011). As we mentioned above, the VCNEB method requires an initial path to be selected. Here, the initial paths of the transition between different phases of Al_2SiO_5 were constructed using the algorithm of Stevanović et al. (Stevanović et al., 2018; Therrien et al., 2020). This algorithm searches for the mapping between the two structures, such that it minimizes the Euclidean distance between the positions of each atom in the initial and final structures. The algorithm consists of two steps. At the first stage, the most convenient representations of the initial and final structures are sought; it allows the optimal representation of unit cells of these structures (Stevanović et al., 2018; Therrien et al., 2020). At this stage, two unit cells are transformed to have the same number of atoms taking into account the total symmetry of nonequivalent supercells whose number is determined within the Hart–Forcade theory (Hart, Forcade, 2008). For each of the two structures, we seek for such unit cell settings (among all possible choices of the unit cell) that are closest to each other. At the second stage, atoms of the structure are placed back into two generated supercells and the algorithm finds such correspondence, or mapping, between the two structures that the total distance traveled by all the atoms from the initial to the final structure be minimal (Stevanović et al., 2018; Therrien et al., 2020). It is important to note that the mapping algorithm is not commutative; thus, for each pair of structures, the algorithm was used to generate two sets of pathways – forth and back (structure A → structure B and structure B → structure A). This geometric approach is crude and there is absolutely no guarantee that the generated path is indeed the optimal one. To increase our confidence that the optimal path is indeed found, for each of the transitions andalusite-kyanite, kyanite-sillimanite and andalusite-sillimanite, we took top ten paths produced by Stevanović algorithm, refined them using VCNEB method and for each transition, took the one with the lowest barrier.

The VCNEB calculations were done using the USPEX code (Oganov, Glass, 2006; Qian et al., 2013) employing forces and stresses calculated using the VASP code (Kresse, Hafner, 1993, 1994; Kresse, Furthmüller, 1996). The VCNEB calculation began with an initial transition path consisting of 20 intermediate structures ("images"). All three polymorphs have 32 atoms in the unit cell, and in all trajectories we considered all intermediate structures also had 32 atoms/cell. For accurate determination of transition states and intermediate minima corresponding to metastable transition states, we used the climbing image–descending image technique (Henkelman et al., 2000). The spring constants for the VCNEB method were varied from 3 to 6 eV/Å^2. The halting criterion for the calculation was set as RMS (Root Mean Square forces) on images that are less than 0.003 eV/Å. Crystal structures were visualized using VESTA software (Momma, Izumi, 2011).

COORDINATION NUMBER ANALYSIS

To understand better these reconstructive transitions, we focused on the changes in the bond network. For the determination of interatomic contacts, we used two approaches.

One approach was based on the Voronoi–Dirichlet partitioning of crystal structures. This is an attractive, unbiased and automatic, way to determine the (integer) coordination number of atom in any crystal structure.

https://www.tandfonline.com/doi/abs/10.1080/08893110412331323170?casa_token=jBJw-5hZxjpIAAAAA:5R-LJpsQ4T3WIDl0At7w2FqrJ0U6pl8ejwSQQnu21TVdRCdR4mofSbZ9Iqn-jx_GhKVTUtaPkFxTJ4pw

Another approach is to use Hoppe's effective coordination number (ECoN) approach (Hoppe, 1979; Hoppe et al., 1989). This approach gives non-integer coordination numbers which change continuously as structure is continuously distorted, and its advantage is its continuous nature, where greater weight is given to stronger interactions. Here, each cation-anion

interaction comes with a weight, in general non-integer. The ECoN approach is based on the exponential decrease of the importance of interatomic contacts with distance.

For a given atom, the ECoN is defined as $\mathrm{ECoN} = \sum_i \omega_i$, where the sum runs over all the atoms in the environment of the chosen central atom. The weight of the i-th atom (ω_i) is defined as:

$$\omega_i = \exp\left[1 - \left(\frac{d_i}{d_{\mathrm{av}}}\right)^6\right], \quad (1)$$

with d_i the distance to atom I and d_{av} the weighted average distance, defined as:

$$d_{\mathrm{av}} \frac{\sum_i d_i \exp\left[1 - \left(\frac{d_i}{d_{\min}}\right)^6\right]}{\sum_i \exp\left[1 - \left(\frac{d_i}{d_{\min}}\right)^6\right]}, \quad (2)$$

where $d_{\min}$ is the shortest distance to the central atom for the considered atomic species.

These two approaches allow us to understand how many interatomic contacts are broken and which new ones are formed during the transition.

RESULTS AND DISCUSSION

Crystal structures of the Al_2SiO_5 phases are shown in Fig. 1*a*–*c*. Gray, orange and green polyhedra shown in Fig. 1*e*–*f* correspond to 6-,5- and 4-coordinate Al atoms. Blue polyhedra in Fig. 1*g* corresponds to silicon atoms, which are 4-fold coordinated in all of these structures.

First, we relaxed structures of all three Al_2SiO_5 phases at the pressures of 0 and 10 GPa. The lowest-enthalpy phase is andalusite at 0 GPa and kyanite at 10 GPa, which is in agreement with experiments and previous calculations (Oganov, Brodholt, 2000). As one can see in Fig. 2, all three phases are energetically close to each other. At 0 GPa, sillimanite is 10 meV/atom higher in energy than andalusite, and kyanite is 12 meV/atom above sillimanite. At 10 GPa, sillimanite is 60 meV/atom higher in enthalpy than kyanite and andalusite is 8 meV/atom above sillimanite.

First, let us consider the transition from andalusite to sillimanite at pressures of 0 and 10 GPa. Both structures have relatively similar orthorhombic cell parameters listed in Table 1. Given the similarity of unit cells and even of crystal structures, one might think that it is trivial to construct the optimal phase transition pathway and that it should be within the orthorhombic cell. We did this both at 0 GPa and 10 GPa, at each pressure constructing the initial pathways by using smooth variation of orthorhombic cell parameters and choosing such mapping of atomic coordinates that minimizes the total distance traveled by all the atoms. Then, we optimized these paths by the VCNEB method. The resulting pathways are presented in Figs. 3 and 4. As one can see, the energy barrier equals 0.389 eV/atom at 0 GPa and 0.353 eV/atom at 10 GPa. It is instructive that these are not the lowest-barrier paths. Considering non-trivial cell mappings, we found lower-barrier paths.

Thus, to describe phase transitions we generated six sets of initial pathways for the optimized structures at each pressure (kyanite → sillimanite, sillimanite → kyanite, kyanite → andalusite, andalusite → kyanite, andalusite → sillimanite and sillimanite → andalusite). The lowest-barrier transition profiles for each transformation at 0 and 10 GPa are shown in Figs. 5 and 6, respectively. For all transitions the symmetry of intermediate states is *P1*. These are all reconstructive phase transitions; barriers for each transition at both pressures are very high and the schemes of transitions with barrier values are presented in Fig. 7. Such high barriers imply that these transitions are kinetically feasible only at high temperatures (the lowest energy barrier is 0.255 eV/atom).

Supporting Materials present the full set of optimized barriers for each kind of transition (10 pathways for A → B and 10 pathways for B → A).

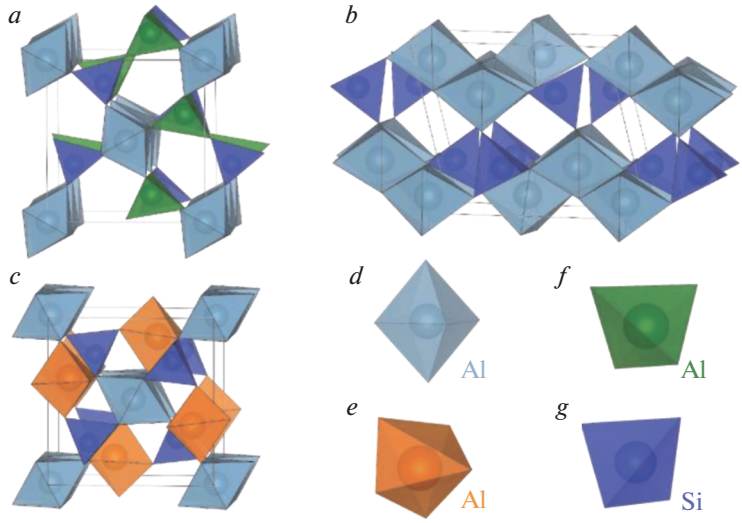

Fig. 1. Crystal structures of (*a*) sillimanite, (*b*) kyanite and (*c*) andalusite phases of Al_2SiO_5. Oxygen atoms are located in the vertices of polyhedra; polyhedra of Al atoms in different structures and correspond to the (*d*) 6-, (*e*) 5- and (*f*) 4-coordinate atoms; (*g*) tetrahedral coordination of Si atom.

Рис. 1. Кристаллические структуры (*a*) силлиманита, (*b*) кианита и (*c*) андалузита фаз Al_2SiO_5. Атомы кислорода расположены в вершинах полиэдров; полиэдры атомов Al в различных структурах соответствуют (*d*) 6-, (*e*) 5- и (*f*) 4-координатным атомам; (*g*) тетраэдрическая координация атома Si.

Looking at the changes of coordination numbers along transition pathways, we found that SiO_4 tetrahedra are preserved during all transitions and there are no changes in the coordination number of silicon. Indeed, Si–O bonds are the strongest here and, naturally, they are perturbed the least. The change of coordination of Al atoms is much more complex and informative – it provides more insights into the transition nature. Figures 8 and 9 show the change of the average coordination number of Al atoms (obtained using Voronoi–Dirichlet partitioning) during all transitions at 0 GPa and 10 GPa, respectively. Figures 10 and 11 present the change of average ECoN of Al atoms during all transitions at 0 GPa and 10 GPa, respectively. Note that the averaging involves all Al atoms (including those which are 6-coordinate in three polymorphs – during transitions, their coordination numbers also change). Transition states have the lowest average coordination number (CN) of Al atoms along the pathway, which is easy to understand – a large number of all Al–O bonds have been broken, while the new ones have not yet been formed.

Table 1. Lattice parameters for orthorhombic structures of andalusite and sillimanite at the pressure of 0 and 10 GPa: theoretical results and experimental data (Ralph et al., 1984; Yang et al., 1997b)

	VASP, 0GPa	Experiment, 0 GPa	VASP, 10 GPa
Andalusite	a = 5.610 Å b = 7.868 Å c = 7.973 Å	a = 5.557 Å b = 7.798 Å c = 7.903 Å	a = 5.534 Å b = 7.647 Å c = 7.821 Å
Sillimanite	a = 5.816 Å b = 7.568 Å c = 7.772 Å	a = 5.777 Å b = 7.488 Å c = 7.681 Å	a = 5.754 Å b = 7.415 Å c = 7.559 Å

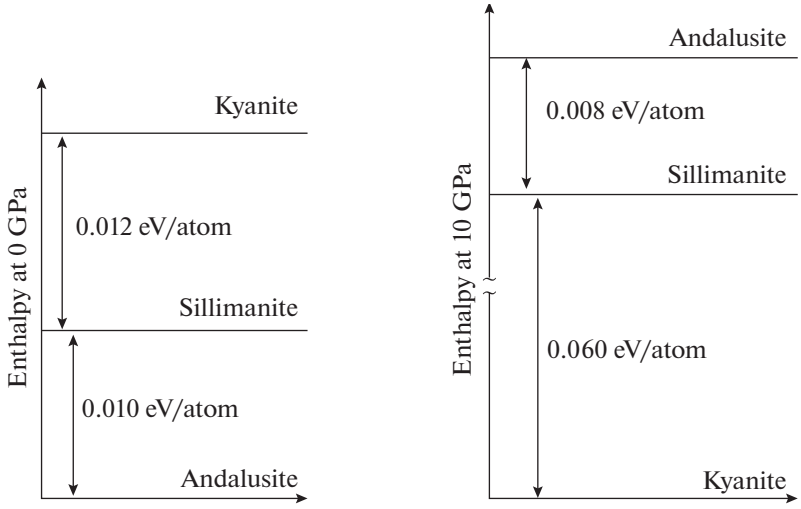

Fig. 2. Enthalpy differences between Al_2SiO_5 phases at 0 GPa and 10 GPa.

Рис. 2. Разности энтальпий между фазами Al_2SiO_5 при 0 и 10 ГПа.

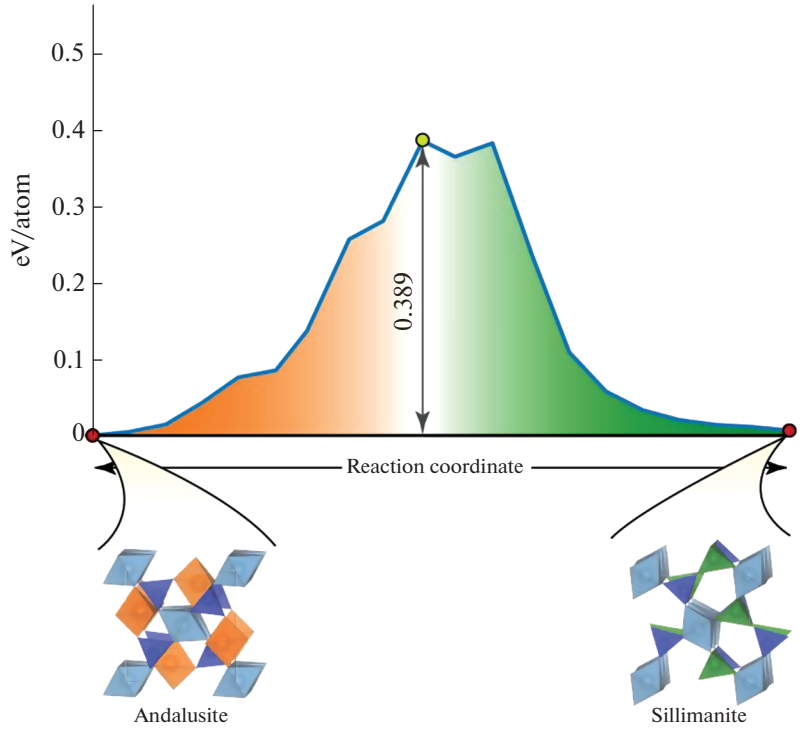

Fig. 3. Enthalpy profile of andalusite-sillimanite transition at 0 GPa for the path involving standard crystallographic unit cells.

Рис. 3. Профиль энтальпии перехода андалузит-силлиманит при 0 ГПа для пути перехода в стандартных кристаллографических элементарных ячейках.

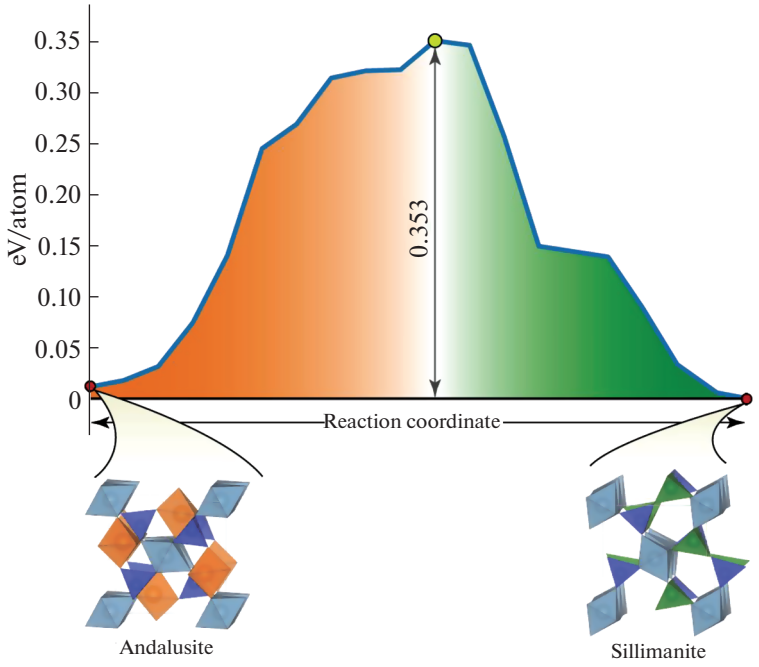

Fig. 4. Enthalpy profile of andalusite-sillimanite transition at 10 GPa for the path involving standard crystallographic unit cells.

Рис. 4. Профиль энтальпии перехода андалузит-силлиманит при 10 ГПа для пути перехода в стандартных кристаллографических элементарных ячейках.

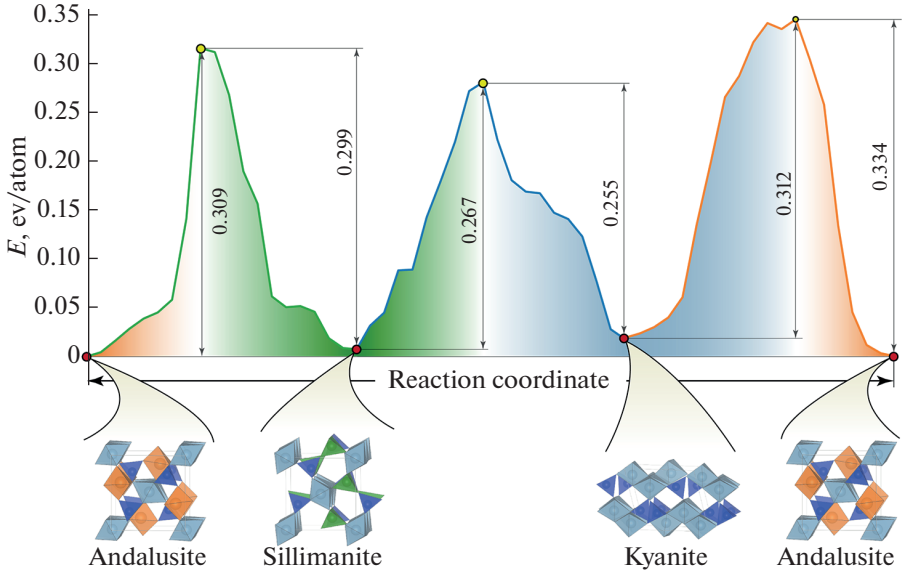

Fig. 5. Enthalpy profile of all three transitions at 0 GPa.

Рис. 5. Профиль энтальпии всех трех переходов при 0 ГПа.

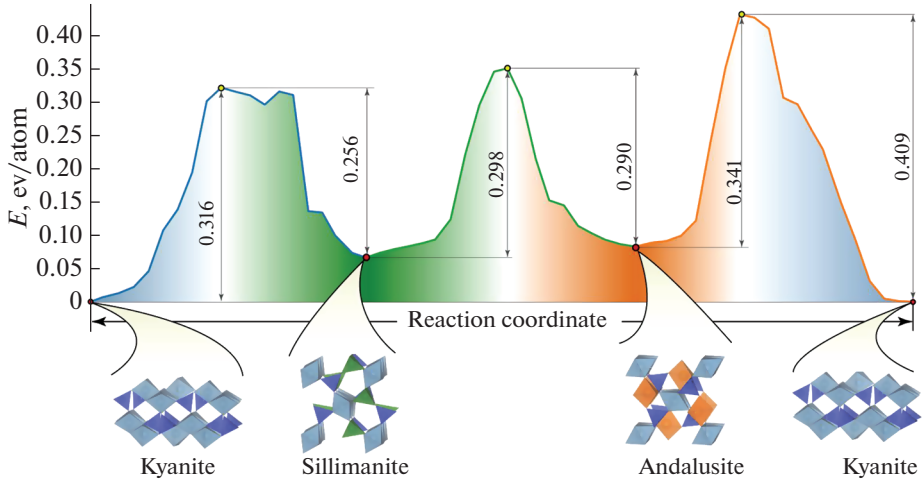

Fig. 6. Enthalpy profile of all three transitions at 10 GPa.

Рис. 6. Профиль энтальпии всех трех переходов при 10 ГПа.

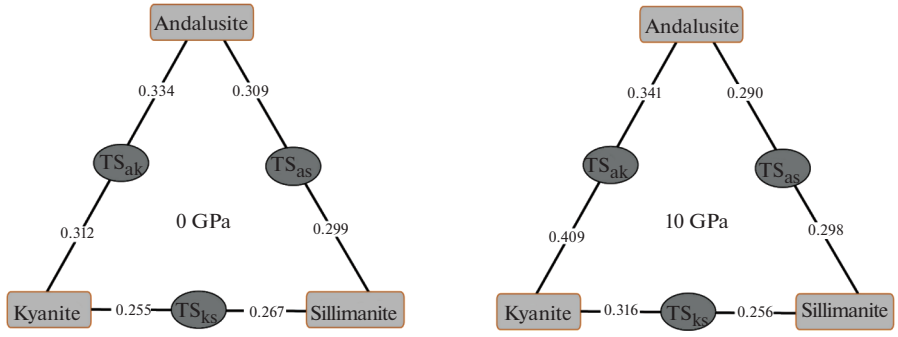

Fig. 7. Calculated enthalpy barriers for transitions at 0 and 10 GPa.

Рис. 7. Рассчитанные энтальпийные барьеры для переходов при 0 и 10 ГПа.

We find that the lowest-barrier transition mechanisms are different at 0 and 10 GPa. For andalusite-sillimanite transition at 0 GPa, the changes of coordination are more complex than at 10 GPa. In general, at high pressure the decrease of the average coordination number in the activated state is smaller.

Two remarks must be made. First, the discussed mechanisms of transitions are the best among those tested, i.e., have the lowest activation barrier and other mechanisms with a lower transition barrier are not excluded since global optimization of phase transition paths was not performed and robust methods for doing so do not exist yet. However, the procedure we use, combining a geometric selection of the "easiest" paths and detailed exploration of these to find the lowest-energy path, should give results close or identical to a full global search. Second, the presented phase transition mechanisms are based on the mean-field approximation, where all unit cells undergo the same changes simultaneously. In reality, first-order phase transitions proceed via nucleation and growth, making the mean-field approximation a rough, but crystallographically and intuitively attractive, model. A more realistic study of nucleation

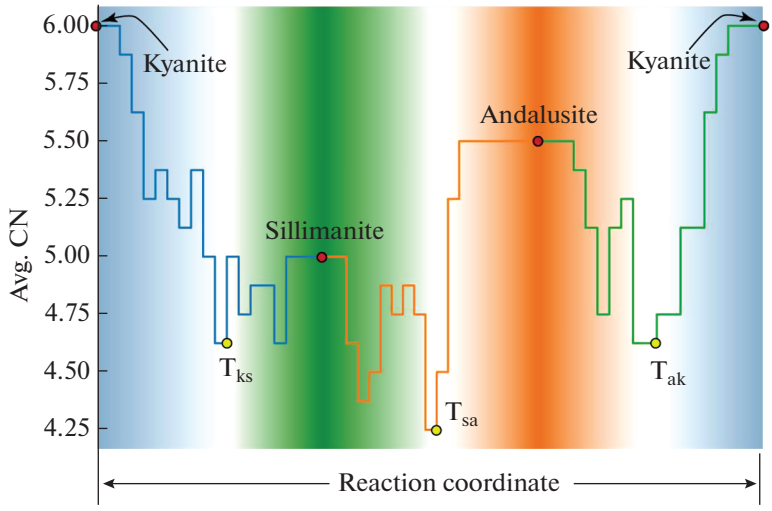

Fig. 8. Average coordination number of Al atoms for all three transitions at 0 GPa.

Рис. 8. Среднее координационное число атомов Al для всех трех переходов при 0 ГПа.

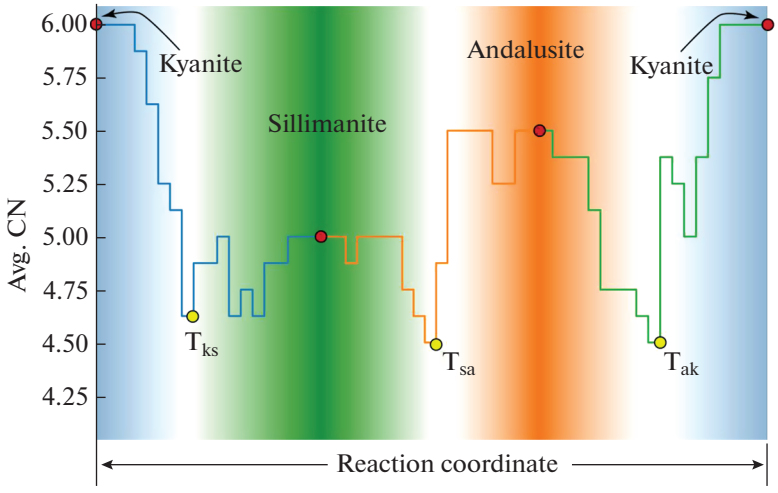

Fig. 9. Average coordination number of Al atoms for all three transitions at 10 GPa.

Рис. 9. Среднее координационное число атомов Al для всех трех переходов при 10 ГПа.

and growth phenomena requires much larger systems (including thousands of atoms) and advanced sampling methods such as transition path sampling (Bolhuis et al., 2002). Transition path sampling method (also implemented in the USPEX code) requires a good mean-field starting model (and our work shows how to obtain it), but this method expensive to be done at *ab initio* level, and requires a very accurate force field – machine learning force fields are promising in this regard.

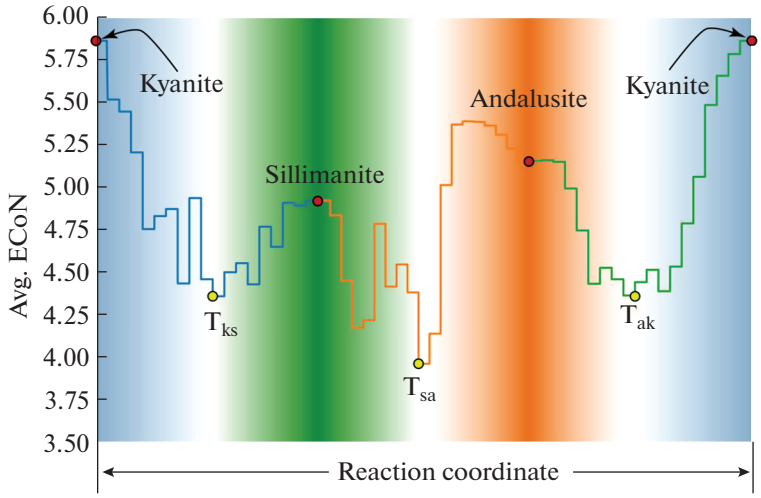

Fig. 10. Average effective coordination number (ECoN) of Al atoms for all three transitions at 0 GPa.
Рис. 10. Среднее эффективное координационное число (ECoN) атомов Al для всех трех переходов при 0 ГПа.

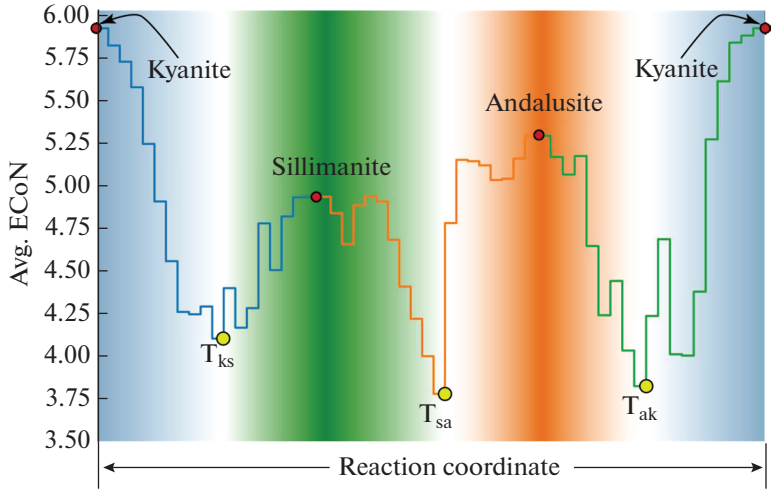

Fig. 11. Average effective coordination number (ECoN) of Al atoms for all three transitions at 10 GPa.
Рис. 11. Среднее эффективное координационное число (ECoN) атомов Al для всех трех переходов при 10 ГПа.

CONCLUSIONS

We show that even if structures are geometrically similar and have similar unit cell parameters (as andalusite and sillimanite), the construction of the transition path is non-trivial and one should not rely on intuitively "obvious" mappings. Moreover, we showed that the mechanism of the same transition changes with pressure. Using state-of-the-art methodologies, we have studied the atomistic mechanisms of phase transitions between the Al_2SiO_5 polymorphs

(andalusite, sillimanite and kyanite) at pressures of 0 and 10 GPa. First, we generated a number of closest mappings between each pair of structures. Then, the variable-cell nudged-elastic-band (VCNEB) method was used for optimizing these paths, allowing us to choose the lowest-barrier path, for which we analyzed the evolution of coordination numbers along the transition path. Our work shows that due to significant changes of coordination numbers (breaking of many bonds), all transitions among Al_2SiO_5 polymorphs have very high barriers, which explains the coexistence of these polymorphs for many millions of years in nature – and that coexistence allows Al_2SiO_5 polymorphs to be widely used for determining P–T-conditions of rock formation.

SUPPORTING INFORMATION AVAILABLE

Detailed description of the evolution of cell parameters during transitions, geometries of transition states and a full set of optimized pathways for each transition (from andalusite to kyanite, from kyanite to sillimanite and from sillimanite to andalusite) at 0 GPa and 10 GPa.

ACKNOWLEDGMENTS

We acknowledge funding from Russian Ministry of Science and Higher Education (grant 2711.2020.2 to leading scientific schools). All calculations were performed on Oleg supercomputer of our laboratory. We thank K.A. Gorskikh for assistance with figures.

REFERENCES

Ali A. The tectono-metamorphic evolution of the Balcooma Metamorphic Group, north-eastern Australia: A multidisciplinary approach. *J. Metamorph. Geol.* **2010**. Vol. 28. P. 397–422.

Allaz J., Maeder X., Vannay J.C., Steck A. Formation of aluminosilicate-bearing quartz veins in the Simano nappe (Central Alps): Structural, thermobarometric and oxygen isotope constraints. *Schweizerische Mineral. und Petrogr. Mitteilungen*. **2005**. Vol. 85. P. 191–214.

Aryal S., Rulis P., Ching W.Y. Density functional calculations of the electronic structure and optical properties of aluminosilicate polymorphs (Al_2SiO_5). *Amer. Miner.* **2008**. Vol. 93. P. 114–123.

Atherton M.P., Brotherton M.S. Metamorphyic index minerals in the Eastern Dalradian. *Scottish J. Geol.* **1974**. Vol. 9. P. 321–324.

Baharfar A.-A., Whitney D.L., Pang K.-N., Chung S.-L., Iizuka Y. Petrology, geothermobarometry, and P–T path of spinel-bearing symplectite migmatites from the Simin area, Hamedan, Sanandaj-Sirjan Zone, Iran. *Turkish J. Earth Sci*. **2019**. Vol. 28. P. 275–298.

Belogurova O.A., Grishin N.N. Carbidized heat insulation materials from kyanite ore. R*efract. Ind. Ceram*. **2012**. Vol. 53. P. 26–30.

Blöchl P.E. Projector augmented-wave method. *Phys. Rev. B.* **1994**. Vol. 50. P. 17953–17979.

Bolhuis P.G., Chandler D., Dellago C., Geissler P.L. Transition path sampling: throwing ropes over rough mountain passes, in the dark. *Annu. Rev. Phys. Chem*. **2002**. Vol. 53. P. 291–318.

Burnham C.W. Refinement of the crystal structure of sillimanite. *Zeit. Krist.* **1963**. Vol. 118. P. 127–148.

Carey J.W., Rice J.M., Grover T.W. Petrology of aluminous schist in the Boehls Butte region of northern Idaho; geologic history and aluminum-silicate phase relations. *Amer. J. Sci.* **1992**. Vol. 292. P. 455–473.

Caspersen K.J., Carter E.A. Finding transition states for crystalline solid-solid phase transformations. *Proc. Natl. Acad. Sci*. **2005**. Vol. 102. P. 6738–6743.

Evans B.W., Bert J.W. Revised metamorphic history for the Chiwaukum Schist, North Cascades, Washington. *Geology*. **1986**. Vol. 14. P. 695.

Eyring H. The activated complex in chemical reactions. *J. Chem. Phys.* **1935**. Vol. 3, P. 63–71.

Garcia-Casco A., Torres-Roldan R.L. Disequilibrium induced by fast decompression in St–Bt–Grt–Ky–Sil–And metapelites from the Betic Belt (Southern Spain). *J. Petrol*. **1996**. Vol. 37. P. 1207–1239.

Gervais F. Three modes of isograd formation in the northern Monashee Complex of the Canadian Cordillera. *Geol. Soc. London, Spec. Publ*. **2019**. Vol. 478. P. 373–388.

Gibson G.M., Peljo M., Chamberlain T. Evidence and timing of crustal extension versus shortening in the early tectonothermal evolution of a Proterozoic continental rift sequence at Broken Hill, Australia. *Tectonics*. **2004**. Vol. 23. TC5012. P. 1–20.

Grover T.W., Rice J.M., Carey J.W. Petrology of aluminous schist in the Boehls Butte region of northern Idaho; phase equilibria and P–T evolution. *Amer. J. Sci*. **1992**. Vol. 292. P. 474–507.

Harben P.W. The industrial minerals handbook: a guide to markets, specifications and prices. Industrial Minerals Information, Ltd., **2002**.

Hart G.L.W., Forcade R.W. Algorithm for generating derivative structures. *Phys. Rev. B – Condens. Matter Mater. Phys*. **2008**. Vol. 77. P. 1–12.

Henkelman G., Jónsson H. Improved tangent estimate in the nudged elastic band method for finding minimum energy paths and saddle points. *J. Chem. Phys*. **2000**. Vol. 113. P. 9978–9985.

Henkelman G., Uberuaga B.P., Jónsson H. A climbing image nudged elastic band method for finding saddle points and minimum energy paths. *J. Chem. Phys*. **2000**. Vol. 113. P. 9901–9904.

Hietanen A. Kyanite, andalusite and sillimanite in the schist in Boels Butte quadrangle, Idaho. *Amer. Miner.* **1956**. Vol. 41. P. 1–27.

Hiroi Y., Kishi S., Nohara T., Sato K., Goto J. Cretaceous high-temperature rapid loading and unloading in the Abukuma metamorphic terrane, Japan. *J. Metamorph. Geol*. **1998**. Vol. 16. P. 67–81.

Hohenberg P., Kohn W. Inhomogeneous electron gas. *Phys. Rev.* **1964** Vol. 136. P. B864–B871.

Hoppe R. Effective coordination numbers (ECoN) and mean fictive ionic radii (MEFIR). *Zeitschrift für Krist. – Cryst. Mater.* **1979**. Vol. 150. P. 23–52.

Hoppe R., Voigt S., Glaum H., Kissel J., Müller H.P., Bernet K. A new route to charge distributions in ionic solids. J. *Less-Common Met.* **1989**. Vol. 156. P. 105–122.

Jonsson H., Mills G., Jacobsen K.W. Nudged elastic band method for finding minimum energy paths of transitions. In: *Classical and Quantum Dynamics in Condensed Phase Simulations*. World Scientific,**1998**. p. 385–404.

Kerrick D.M. The Al_2SiO_5 polymorphs. Walter de Gruyter GmbH & Co KG, **2018**.

Kim H.S., Ree J.H. P-T modeling of kyanite and sillimanite paramorphs growth after andalusite in late Paleozoic Pyeongan Supergroup, South Korea: Implication for metamorphism during the Mesozoic tectonic evolution. *Lithos*. **2010**. Vol. 118. P. 269–286.

Klein C., Hurlbut C. Manual of mineralogy (by James D. Dana). **1995**.

Kohn W., Sham L.J., Self-consistent equations including exchange and correlation effects. *Phys. Rev.* **1965**. Vol. 140. P. A1133–A1138.

Kresse G., Furthmüller J. Efficient iterative schemes for ab initio total-energy calculations using a plane-wave basis set. *Phys. Rev. B.* **1996**. Vol. 54. P. 11169–11186.

Kresse G., Hafner J. Ab initio molecular-dynamics simulation of the liquid-metalamorphous- semiconductor transition in germanium. *Phys. Rev. B.* **1994**. Vol. 49. P. 14251–14269.

Kresse G., Hafner J. Ab initio molecular dynamics for liquid metals. *Phys. Rev. B.* **1993**. Vol. 47. P. 558–561.

Kresse G., Joubert D. From ultrasoft pseudopotentials to the projector augmented-wave method. *Phys. Rev. B.* **1999**. Vol. 59. P. 1758–1775.

Likhanov I.I., Reverdatto V.V., Kozlov P.S., Popov N.V. Kyanite–sillimanite metamorphism of the Precambrian complexes, Transangarian region of the Yenisei Ridge. *Russ. Geol. Geophys*. **2009**. Vol. 50. P. 1034–1051.

Lux D.R., DeYoreo J.J., Guldotti C.V., Decker E.R. Role of plutonism in low-pressure metamorphic belt formation. *Nature*. **1986**. Vol. 323. P. 794–797.

McMichael B. Aluminosilicate minerals. Refractories steel the Show. *Ind. Miner.* **1990**. P. 27–43.

Momma K., Izumi F. VESTA 3 for three-dimensional visualization of crystal, volumetric and morphology data. *J. Appl. Crystallogr.* **2011**. Vol. 44. P. 1272–1276.

Monkhorst H.J., Pack J.D. Special points for Brillouin-zone integrations. *Phys. Rev. B.* **1976**. Vol. 13. P. 5188–5192.

Munro J.M., Akamatsu H., Padmanabhan H., Liu V.S., Shi Y., Chen L.Q., Vanleeuwen B.K., Dabo I., Gopalan V. Discovering minimum energy pathways via distortion symmetry groups. *Phys. Rev. B.* **2018**.

Oganov A.R., Brodholt J.P. High-pressure phases in the Al_2SiO_5 system and the problem of aluminous phase in the Earth's lower mantle: ab initio calculations. *Phys. Chem. Miner.* **2000**. Vol. 27. P. 430–439.

Oganov A.R., Glass C.W. Crystal structure prediction using ab initio evolutionary techniques: Principles and applications. *J. Chem. Phys.* **2006**. Vol. 124. P. 1–15.

Oganov A.R., Lyakhov A.O., Valle M. How evolutionary crystal structure prediction works – and why. *Acc. Chem. Res.* **2011**. Vol. 44. P. 227–237.

Oganov A.R., Ma Y., Lyakhov A.O., Valle M., Gatti C. Evolutionary crystal structure prediction as a method for the discovery of minerals and materials. *Rev. Miner. Geochem*. **2010**. Vol. 71. P. 271–298.

Oganov A.R., Price G.D., Brodholt J.P. Theoretical investigation of metastable Al_2SiO_5 polymorphs. *Acta Crystallogr. Sect. A Found. Crystallogr.* **2001**. Vol. 57. P. 548–557.

Ohuchi F.S., Ghose S., Engelhard M.H., Baer D.R. Chemical bonding and electronic structures of the Al_2SiO_5 polymorphs, andalusite, sillimanite, and kyanite: X-ray photoelectron-and electron energy loss spectroscopy studies. *Amer. Miner.* **2006**. Vol. 91. P. 740–746.

Palin R.M., Searle M.P., Waters D.J., Horstwood M.S.A., Parrish R.R. Combined thermobarometry and geochronology of peraluminous metapelites from the Karakoram metamorphic complex, North Pakistan; New insight into the tectonothermal evolution of the Baltoro and Hunza Valley regions. *J. Metamorph. Geol.* **2012**. Vol. 30. P. 793–820.

Pattison D.R.M., Tracy R.J., Kerrick D.M. Contact metamorphism. In: *Contact Metamorphism*. Ed. D.M. Kerrick. Rev. Miner. Ceochem. P. 105–206.

Perdew J.P., Burke K., Ernzerhof M. Generalized gradient approximation made simple. *Phys. Rev. Lett.* **1996**. Vol. 77. P. 3865–3868.

Qian G., Dong X., Zhou X., Tian Y., Oganov A.R., Wang H.-T. Variable cell nudged elastic band method for studying solid–solid structural phase transitions. *Comput. Phys. Commun*. **2013**. Vol. 184. P. 2111–2118.

Ralph R.L., Finger L.W., Hazen R.M., Ghose S. Compressibility and crystal structure of andalusite at high pressure. *Amer. Miner*. **1984**. Vol. 69. P. 513–519.

Sayab M. Decompression through clockwise P-T path: implications for early N-S shortening orogenesis in the Mesoproterozoic Mt Isa Inlier (NE Australia). *J. Metamorph. Geol*. **2006**. Vol. 24. P. 89–105.

Schmidt M.W., Poli S., Comodi P., Zanazzi P.F. High-pressure behavior of kyanite: Decomposition of kyanite into stishovite and corundum. *Amer. Miner*. **1997**. Vol. 82. P. 460–466.

Schneider H., Komarneni S. Basic properties of mullite, in: *Mullite.* Wiley Online Library, **2005**. P. 141–155.

Schneider H., Schreuer J., Hildmann B. Structure and properties of mullite – a review. *J. Eur. Ceram. Soc.* **2008**. Vol. 28. P. 329–344.

Sepahi A.A., Whitney D.L., Baharifar A.A. Petrogenesis of andalusite-kyanite-sillimanite veins and host rocks, Sanandaj-Sirjan metamorphic belt, Hamadan, Iran. *J. Metamorph. Geol*. **2004**. Vol. 22. P. 119–134.

Sheppard D., Xiao P., Chemelewski W., Johnson D.D., Henkelman G. A generalized solid-state nudged elastic band method. *J. Chem. Phys*. **2012**. Vol. 136. P. 074103.

Skoog A.J., Moore R.E. Refractory of the past for the future: mullite and its use as a bonding phase. *Amer. Ceram. Soc. Bull.* **1988**. Vol. 67. P. 1180–1185.

Stevanović V., Trottier R., Musgrave C., Therrien F., Holder A., Graf P. Predicting kinetics of polymorphic transformations from structure mapping and coordination analysis. *Phys. Rev. Mater.* **2018**. Vol. 2. P. 033802.

Therrien F., Graf P., Stevanović V. Matching crystal structures atom-to-atom. *J. Chem. Phys.* **2020**. Vol. 152.

Whitney D.L. Coexisting andalusite, kyanite, and sillimanite: Sequential formation of three Al_2SiO_5 polymorphs during progressive metamorphism near the triple point, Sivrihisar, Turkey. *Amer. Miner.* **2002**. Vol. 87. P. 405–416.

Whitney D.L., Samuelson W.J. Crystallization sequences of coexisting andalusite, kyanite, and sillimanite, and a report on a new locality: Lesjaverk, Norway. *Eur. J. Miner*. **2019**. Vol. 31. P. 731–737.

Yang H., Downs R.T., Finger L.W., Hazen R.M., Prewitt C.T. Compressibility and crystal structure of kyanite, Al_2SiO_5, at high pressure. *Amer. Miner*. **1997a**. Vol. 82. P. 467–474.

Yang H., Hazen R.M., Finger L.W., Prewitt C.T., Downs R.T. Compressibility and crystal structure of sillimanite, Al_2SiO_5, at high pressure. *Phys. Chem. Miner*. **1997b**. Vol. 25. P. 39–47.

Zhang W., Meng Q., Dai W. Research on application of kyanite in plastic refractory. *Chinese J. Geochem*. **2013**. Vol. 32. P. 326–330.

Zhu Q., Oganov A.R., Lyakhov A.O. Evolutionary metadynamics: a novel method to predict crystal structures. *Cryst. Eng. Comm*. **2011**. P. 1–7.

МЕХАНИЗМЫ ФАЗОВЫХ ПЕРЕХОДОВ В ПОЛИМОРФАХ Al_2SiO_5

А. И. Самцевич[a], *, А. Р. Оганов[a], **

[a] *Сколковский институт науки и технологий, Большой бульв., 30, стр. 1, Москва, 121205 Россия*

**e-mail: A.Samtsevich@skoltech.ru,*

***e-mail: A.Oganov@skoltech.ru*

Поступила в редакцию 26.05.2021 г.

После доработки 07.07.2021 г.

Принята к публикации 18.08.2021 г.

В природе Al_2SiO_5 существует в виде трех полиморфов: кианита, андалузита и силлиманита, которые часто сосуществуют в одной и той же породе. В этой работе мы подробно изучили механизмы структурных фазовых переходов между всеми тремя фазами Al_2SiO_5 – кианит-андалузитом, андалузит-силлиманитом и кианит-силлиманитом при давлениях 0 и 10 ГПа. Пути фазового перехода с наименьшими энергетическими барьерами найдены путем построения ряда наиболее геометрически выгодных путей и их оптимизации с помощью метода упругой ленты с варьируемой ячейкой (VCNEB). В результате мы получаем представление о природе структурных изменений между полиморфами Al_2SiO_5, сосуществовании фаз друг с другом и путях превращения.

Ключевые слова: полиморфы Al_2SiO_5, механизмы фазовых переходов, теория функционала плотности